

DYNAMIC AUTOTUNING OF ADAPTIVE FAST MULTIPOLE METHODS ON HYBRID MULTICORE CPU & GPU SYSTEMS

MARCUS HOLM, STEFAN ENGBLOM, ANDERS GOUDE, AND SVERKER HOLMGREN

ABSTRACT. We discuss an implementation of adaptive fast multipole methods targeting hybrid multicore CPU- and GPU-systems. From previous experiences with the computational profile of our version of the fast multipole algorithm, suitable parts are off-loaded to the GPU, while the remaining parts are threaded and executed concurrently by the CPU. The parameters defining the algorithm affects the performance and by measuring this effect we are able to dynamically balance the algorithm towards optimal performance. Our setup uses the dynamic nature of the computations and is therefore of general character.

1. INTRODUCTION

The N -body simulation is an ubiquitous problem in computational science, arising in many different application areas and attracting a lot of interest from developers of numerical algorithms and software for many years. For the computation of interaction forces, the naive all-pairs algorithm scales as $\mathcal{O}(N^2)$, and approximative algorithms have been developed with better asymptotic computational complexity. For large N -body problems requiring accurately determined forces it is known that the Fast Multipole Method (FMM) [6, 17] is more efficient (in terms of the number of arithmetic operations required) than both the all-pairs algorithm and more classic tree-based schemes like the Barnes-Hut algorithm [4, 14].

About a decade ago, physical constraints in chip design spawned a paradigm shift in computer architecture. Increased performance is now realized mainly by increased thread parallelism rather than increased clock speed. Also, the instruction complexity and the memory/communication bandwidth is increasing at a significantly slower rate than the computational performance. This implies that other aspects than arithmetic complexity need to be assessed when designing numerical algorithms, prominently parallelism and locality of data access. In this context, FMM algorithms have the potential of becoming increasingly important tools for CSE applications since they combine optimal $\mathcal{O}(N)$ complexity with potential for large-scale parallelism and large amounts of spatial and temporal data locality. However, parallelizing and localizing the FMM computations to make them suitable for modern computer hardware is a non-trivial task, and has also received considerable attention lately [7, 11, 16, 24, 25].

Date: March 17, 2014.

2010 Mathematics Subject Classification. Primary: 65Y05; Secondary: 65Y10.

Key words and phrases. adaptive fast multipole method, task-based, CUDA, graphics processing units, autotuning, load-balancing.

Corresponding author: S. Engblom, telephone +46-18-471 27 54, fax +46-18-51 19 25.

In this paper we present a recently developed variant of the FMM [15, 16] and show that it can be efficiently adapted for parallelization on modern computer systems. We exploit the heterogeneity inherent in the algorithm to compose a highly effective yet flexible hybrid parallel FMM scheme which exploits both multiple CPU threads and an accelerator. By using a dynamic autotuning technique, our implementation can exploit systems with different hardware characteristics and adapt to different problem settings without the need for explicitly modifying a large set of computer architecture- and problem-dependent parameters. The algorithm also achieves good performance on dynamic problems that change characteristics dramatically over time. We argue that the approach of basing implementations on heterogeneous computer systems on a hybrid approach using the inherent heterogeneity of *the algorithm* can be very fruitful for many other computational science kernels, apart from the FMM.

In Section 2 we summarize our version of the adaptive FMM and also briefly discuss the computational complexity. The hybrid parallelization is described in some detail, including complexity estimates, in Section 3. Our autotuning approach is presented in Section 4, where we design several autotuning regulators in an incremental way. One important aspect is that we want a black-box regulator not requiring explicit complexity estimates. Also, we devise an autotuning scheme where the extra work performed for tuning is limited by a parameter - essentially the only parameter that is explicitly needed from the user. In Section 5 we perform computational experiments for our parallel implementation of a 2D FMM and show that the suggested autotuning algorithm provides good performance for problems from different classes, including those whose characteristics change dynamically. A concluding discussion is found in Section 6.

2. FAST MULTIPOLE METHODS

Since first presented in [6, 17], Fast Multipole Methods (FMMs) have remained a crucial tool for fast evaluation of pairwise interactions of the type

$$(2.1) \quad \Phi(x_i) = \sum_{j=1, j \neq i}^N G(x_i, x_j), \quad x_i \in \mathbf{R}^D, \quad i = 1 \dots N,$$

where $D \in \{2, 3\}$ and where the kernel G satisfies suitable growth- and regularity assumptions [15]. Up to some specified tolerance, the FMM algorithm produces a representation of the field $\Phi(y)$ due to the N *sources* $\{x_j\}$ enclosed in some finite domain (the terms *potentials* and *particles* will also be used). Hence a slightly more general viewpoint is that the FMM makes it possible to efficiently evaluate

$$(2.2) \quad \Phi(y_i) = \sum_{j=1, x_j \neq y_i}^N G(y_i, x_j), \quad i = 1 \dots M,$$

in which the effect of the sources $\{x_j\}$ is to be measured in a set of *evaluation points* $\{y_i\}$. In this section we briefly describe the version of FMMs considered in this paper (see [15, 16] for earlier accounts).

2.1. Well-separated sets. FMMs are all based on the observation that the field experienced from distant potentials can be approximated effectively. Generally, let a collection of potentials be organized in two disjoint boxes with radii r_1 and r_2 ,

and let those boxes be separated at a distance d . For quite general non-oscillating kernels G , one can then show that the correct interpretation of ‘distant’ is that [15],

$$(2.3) \quad R + \theta r \leq \theta d,$$

where $R = \max\{r_1, r_2\}$, $r = \min\{r_1, r_2\}$, and $\theta \in (0, 1)$ a certain parameter which controls the accuracy. Eq. (2.3) is the θ -criterion and the two boxes are said to be *well-separated* whenever it applies. If this is so, then the interactions can be compressed and handled as one single operation (or *shift*) between the boxes. If the criterion does not apply, then the boxes are split into smaller boxes until they either are small enough that (2.3) applies, or until they contain a sufficiently small number of potentials that the interactions can be computed directly.

This recursive way of iteratively dividing the source points makes a tree-based approach natural, where each level in the *multipole tree* contains a collection of boxes. Initially, all potentials are understood to be organized into a single box at the 0th level in the tree. Recursively one then splits the boxes into smaller boxes (“children”) such that the number of points per box decreases. Following the prescription in [15], a pairwise relation between all boxes at the same level in the tree is now defined. Boxes are said to be either *strongly* or *weakly coupled*, or they are *decoupled*. Firstly, a box is defined to always be strongly connected to itself. Secondly, boxes obtained by splitting strongly connected boxes are by default also strongly connected. *However*, if two such boxes happen to satisfy the θ -criterion, then they become weakly coupled. Finally, children of weakly coupled boxes are defined to be decoupled. The result of this way of handling the multipole mesh is visualized in Figure 2.1 where two examples of connectivity patterns are displayed.

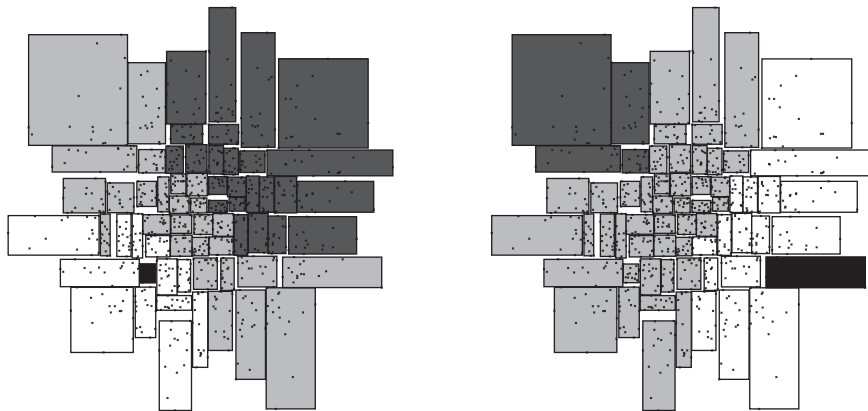


FIGURE 2.1. The different types of connections in an adaptive mesh. The target box is colored in black and *strongly connected* boxes are white. The other boxes are *well-separated* from the target box (they satisfy the θ -criterion (2.3)). The boxes in light gray are *weakly coupled* and interact through M2L interactions at this level in the multipole tree, while the boxes in dark gray are *decoupled* and has already been accounted for at a coarser level in the multipole tree.

At all levels in the multipole tree, the boxes have an *outgoing* and an *ingoing* expansion. The former, also referred to as a *multipole expansion*, represents the effect of potentials enclosed in the box and is accurate in boxes which are well-separated from the current box. The latter is instead a *local expansion* and captures the effect of distant well-separated boxes within the current box.

The computational part of the FMM algorithm is depicted schematically in Figure 2.2. Characteristically, one proceeds in an *upward* and a *downward* phase. In the first phase, the *multipole-to-multipole* (M2M) operation propagates outgoing expansion upwards in the tree. In the second phase, the *multipole-to-local* (M2L) and the subsequent *local-to-local* (L2L) operation translates and propagates this field into local expansions downwards in the tree. Any remaining potentials not accounted for through these operations are handled by direct evaluation of (2.1) at the finest level in the tree.

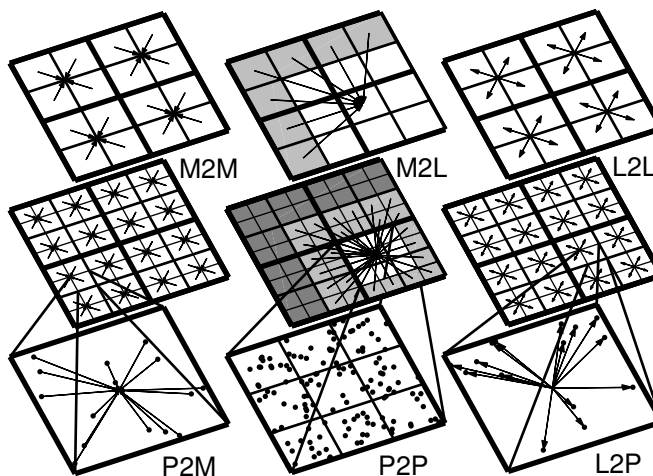


FIGURE 2.2. A schematic view of the FMM algorithm; see text for further details. *Left*: Initialization using Particle-to-Multipole (P2M) shifts, and in the upward phase, Multipole-to-Multipole (M2M) shifts. *Middle and right*: (downward phase) Multipole-to-Local (M2L), followed by Local-to-Local (L2L) shifts. *Bottom*: The direct Particle-to-Particle (P2P) interaction and the Local-to-Particle (L2P) provides for the final evaluation of the potential field.

2.2. The balanced adaptive FMM. When the FMM algorithm is described as above it makes no assumptions on the precise way the boxes that make up the multipole mesh are to be constructed. A standard implementation uses a tree data structure with a locally adapted depth, resulting in a rather complex communication pattern including several levels in the trees. An alternative formulation is presented in [15], where a *balanced tree* (or a *pyramid* data structure) is used instead of a general tree. This introduces additional structure in the algorithm, making parallelization easier and avoids communications across several levels in the multipole

tree. In order to balance the cost of the direct evaluation at the finest level, splitting the boxes close to the median value ensures an almost equal number of points in each box. For more details, consult the distributed source code directly (see Section 6.1). We refer to this FMM version as the *balanced* FMM algorithm. This scheme has previously been implemented for 2D FMMs on a GPU [16], showing good scalability and indeed indicating a potential for efficient implementation also on other parallel architectures.

2.3. Complexity. Most experience suggests that the practical complexity of the FMM algorithm is $\mathcal{O}(N)$ [5], but it has been pointed out that certain special distribution of points may imply a quadratic complexity [1]. To get some feeling for the computational complexity of the balanced FMM algorithm we first consider a 2D setting and a collection of N uniformly distributed particles in the unit square. Let the FMM algorithm be parametrized by the parameter pair $(N_{\text{levels}}, \theta)$. Then the dominating computational work is done at the finest level in the multipole tree and amounts to (i) the M2L shifts, and (ii) the direct P2P interactions.

Since the tree is a balanced quad-tree, the number of boxes at the finest level is explicitly given by $N_f = 4^{N_{\text{levels}}-1}$. Our simplifying assumption of a uniform particle distribution implies that the boxes are approximately uniform in size. Hence the radii are given by

$$(2.4) \quad r \sim 1/\sqrt{2N_f},$$

and also

$$(2.5) \quad r_{\text{parent}} \sim 2r,$$

where r_{parent} is the radius at the second finest level. Similarly, the average area of a box at the finest level is given by $a := 1/N_f$ and the number of source points per box by $n_p := N/N_f$. Thanks to the type of adaptivity used we note that the latter estimate is independent of the details of the distribution of points.

Consider first the arithmetic cost of the direct interaction (P2P). Since we have assumed the radii to be approximately uniformly distributed, $R \sim r$ in (2.3), and hence the boundary for direct interaction is found at $d \sim (1 + \theta)/\theta \times r$. With an area density of potentials $\rho := n_p/a$ we get, since in each of N_f boxes, n_p points are to interact with all points in a circle of radius about d , that the total complexity can be estimated by

$$(2.6) \quad \begin{aligned} C_{\text{P2P}} &\sim N_f \times \pi d^2 \rho \times n_p \\ &\sim \frac{N^2}{2N_f} \times \pi[(1 + \theta)/\theta]^2. \end{aligned}$$

Next we take the cost of the M2L-shift into account. Using p terms in both the outgoing and the ingoing expansions, we have that the M2L-interaction is a linear mapping between p coefficients, and hence has complexity p^2 . This mapping is performed in N_f boxes provided that the θ -criterion is true at the finest level, but false at the second finest level. This can be written as

$$(2.7) \quad \begin{aligned} C_{\text{M2L}} &\sim N_f \times \pi(d_{\text{parent}}^2 - d^2)/a \times p^2 \\ &\sim \frac{3N_f}{2} p^2 \times \pi[(1 + \theta)/\theta]^2, \end{aligned}$$

where by the same argument as before $d_{\text{parent}} \sim (1 + \theta)/\theta \times r_{\text{parent}}$. Note that the *total* cost of M2L at all levels forms a geometric series in terms of the work done at the finest level. Hence the total complexity can be estimated to be $(1 + 1/4 + 1/16 + \dots) \times C_{\text{M2L}} \leq 4/3 \times C_{\text{M2L}}$.

For completeness, let us also briefly discuss the other operations in the FMM-algorithm. Thanks to the pyramid data-structure we readily see that regardless of the distributions of points we always have for the *total* costs that

$$(2.8) \quad C_{\text{M2M}} \sim C_{\text{L2L}} = (1 + 1/4 + 1/16 + \dots) \times N_f \times p^2 \leq 4/3 \times N_f p^2,$$

and also trivially,

$$(2.9) \quad C_{\text{P2M}} \sim C_{\text{L2P}} \sim Np.$$

With a specified relative tolerance TOL, we have that $p \sim \log \text{TOL} / \log \theta$ (see [15]), so that by choosing $N_f \propto N$, the total complexity can be expected to be bounded by a constant times $\theta^{-2} \log^{-2} \theta \cdot N \log^2 \text{TOL}$.

For a 3D FMM, the estimates corresponding to (2.6)–(2.7) are

$$(2.10) \quad C_{\text{P2P}} \sim \frac{3^{1/2} N^2}{2N_f} \times \pi[(1 + \theta)/\theta]^3,$$

$$(2.11) \quad C_{\text{M2L}} \sim \frac{7 \cdot 3^{1/2} N_f}{2} p^4 \times \pi[(1 + \theta)/\theta]^3,$$

where the factor p^4 can be improved to p^3 , or even p^2 , depending on the implementation [8]. The total complexity is in any case now bounded by a constant times $\theta^{-3} \log^{-4} \theta \cdot N \log^4 \text{TOL}$.

3. PARALLELIZATION

In this section, we describe an efficient and robust parallel FMM algorithm for a heterogeneous computational node with several CPU threads and a hardware accelerator in the form of a GPU. This is the standard architecture for laptop and desktop computers and also the standard building block in larger, more specialized computers aimed at solving large-scale computational science and engineering problems. An efficient single-node algorithm is clearly an essential building-block when devising an implementation on multi-node distributed computer systems. In Section 5 we present results from an implementation of our autotuned parallel algorithm for a 2D FMM. As we will clarify later, the parallelization scheme is applicable also to 3D settings, using the same basic data structures and autotuning techniques.

3.1. The parallel FMM algorithm for a hybrid node architecture. Devising algorithms for efficient utilization of a heterogeneous computer architecture is a challenging task. New hardware is continuously developed and released, and there is a need for algorithms that can easily be made efficient also on nodes with new processors and accelerators. The algorithms should automatically adapt to the specifics of new hardware, without the need for a user to provide computer system-dependent parameters. In the same way, the algorithm should be robust to changes in the problem setting, relieving the user also of the task of modifying problem-dependent parameters. Combined with the autotuning scheme discussed in Section 4, the parallel FMM algorithm presented below fulfills these criteria. The

algorithm presented can be very useful for performing practical FMM computations in applications.

The balanced FMM algorithm has previously been implemented in a GPU-only code [16]. Here, good speedup is achieved compared to a well-optimized single-core CPU implementation. However, not every stage of the algorithm is equally well-suited for execution on the GPU, and some stages are also independent and can be executed in parallel. These are also the main observations forming the basis for our new parallel FMM algorithm for hybrid architectures. First we note that the most demanding stages in the FMM, the downward pass and the direct near-field evaluations, are independent of each other. This means that we can offload the near-field evaluations to the accelerator while the downward pass is simultaneously completed on the CPU. This pre-defined scheduling of the work is motivated by the fact that small all-pairs N -body problems can be solved extremely efficiently on accelerators, see e.g. [21], while the hierarchical FMM operations can be considered to be better suited for a general-purpose processor, at least in the sense of coding complexity [16].

The pyramid data-structure used in the balanced FMM allows us to easily parallelize the downward pass in the algorithm using a task-based parallelization model. Here, a main task starts to work at the root of the tree and is allowed to continue in a breadth-first fashion until it reaches a certain predefined level. The main task then creates one subtask per parent node at this level. The number of potential tasks grows rapidly after each level, and the initial serial work can in general be ignored for an implementation on a multithreaded CPU. Because of the connectivity guaranteed by our partitioning scheme, each task created in this way is independent of the other tasks and completes the downward pass for one branch of the tree. In this way, it is possible to launch a number of subtasks that is appropriate for the CPU and create work units with suitable granularity and memory footprint to ensure good load balance and cache utilization.

The original formulation of the FMM algorithm explicitly calculates $G(x_i, x_j)$ and $G(x_j, x_i)$ simultaneously, halving the number of interactions to be computed. However, this symmetry introduces a dependency in the downward pass that requires task synchronization on every level. In a task-based parallel framework it is possible to implement this with a minimum of communication, but experiments using the implementation described below showed that this still results in poor scaling. Hence, in the current implementation, both $G(x_i, x_j)$ and $G(x_j, x_i)$ are calculated explicitly, increasing the number of arithmetic operations but removing the need for synchronization at all FMM tree levels.

With the two heaviest components of the FMM algorithm being executed simultaneously by the CPU and the accelerator, the work for partitioning the particles and initializing the finest level of the tree (P2M) becomes significant. Here, particle partitioning is easily parallelizable in the same way as the downward pass while the P2M step is embarrassingly parallel and can be parallelized accordingly.

In the near-field evaluation (P2P), the contribution from all boxes within the near-field of a box should be calculated at all evaluation points of the box. Similar to the M2L translations, the number of boxes in the near-field varies due to the adaptivity. On a multithreaded CPU, the parallelization is trivial. On a GPU-like accelerator, parallelization is also easy but more work is needed to ensure locality and efficient use of the GPU memory.

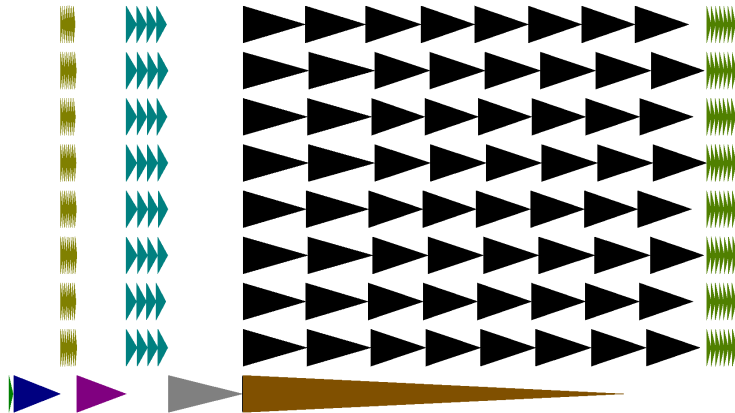


FIGURE 3.1. SuperGlue Execution Visualizer display for a typical run with eight worker threads and a GPU. Triangles correspond to tasks, and are executed from left to right. Each row represents one thread, starting with the master thread at the bottom. The parallel sections correspond to the initial topological phase (light green), the P2M- (cyan), the M2L- (black), and the L2P-shifts (green), respectively. The long brown arrow represents the main thread waiting while the P2P step executes on the GPU.

In [7], an efficient FMM algorithm for a multithreaded CPU is described and implemented. Compared to the work presented there, we have chosen a slightly different parallelization strategy. In [7], the tree construction is left serial, a choice motivated by the fact that in some applications it may be possible to amortize this cost. We chose to parallelize the particle partitioning phase of tree construction, partly because our balanced FMM algorithm involves slightly more work for this stage, but also because there are many applications in which tree construction is done for every (or almost every) force computation and amortizing is not efficient. We also made the choice to leave the upward pass serial since this operation is less demanding in our implementation than in the FMM variant in [7] and since we do not expect this step to become a significant performance bottleneck on hardware available in the foreseeable future (see the length of the gray arrow in Figure 3.1).

3.2. Implementation on a hybrid architecture. Today, there is a plethora of different programming tools for heterogeneous computer systems, still without a clear standard emerging. To handle this situation, a clear separation between algorithm and implementation is needed and algorithms should be easy to implement using different programming tools. However, to be able to perform numerical experiments and performance tests, it is clear that a choice of programming models must be made. The current parallel implementation of our FMM algorithm uses a task-based parallelization approach implemented using the SuperGlue library [23]. In task-based programming, a number of worker threads is created at program initialization and execute tasks that are submitted to a scheduler dynamically. There are other task-based programming libraries that are designed with hybrid architectures in mind, for example StarPU [3]. Here, a black-box approach is taken, where

the scheduler is used to execute a given set of tasks in an efficient way, without taking any specifics of the underlying algorithm into account. StarPU is able to choose among hardware resources and select where to schedule tasks so the total runtime will be small. For example, if a relatively fast GPU has a long queue of tasks already scheduled, StarPU may decide to give a task to a relatively slow CPU thread instead. Hence, a tool like StarPU works with a static algorithm that produces a set of tasks that are dynamically scheduled and executed. In contrast, our approach is to tune the *algorithm* itself dynamically, producing a mixture of tasks that can be efficiently executed on a heterogeneous machine essentially without requiring a unified task library.

Our current FMM implementation assumes the use of a GPU accelerator, and the accelerator code is written using Nvidia Cuda 2.0 [20]. As indicated above, we realize that for future implementations, another task-based programming model and/or another other programming tool for the accelerator should possibly be used.

3.3. Parallel efficiency and attainable performance. Before we describe our methods for autotuning, we will show that our FMM implementation is efficient and achieves satisfactory hardware utilization. The tests described below were performed using the hardware configuration described in Section 5.

The work in [7] provides a good reference for comparison when using only a multithreaded CPU. In [7], good speedup for the P2P phase on up to 8 threads on an Intel Nehalem is achieved. However, the other computationally heavy phases show speedups between about 3.2x (for M2L) and 5x (for M2M and P2M). Figure 3.2 shows the speedup for our implementation for up to 8 threads and for a problem with a million uniformly distributed particles. It is clear that the speedup is perfect for the P2P phase, and about 6–7x for most other phases. The partitioning step of tree construction suffers from a non-optimal data access pattern and is bandwidth-bound, resulting in a maximum speedup of 2.3x. The total speedup on 8 threads for the full multithreaded algorithm is 6.26x.

In [16] it was shown that the P2P phase of our algorithm can run up to 12x faster on an Nvidia Tesla C2075 GPU compared to a single Intel Xeon W3680 core, and the code as a whole ran about 10x faster on the GPU. A straight comparison with those results is not appropriate because the codes are optimized differently (for example, to reduce the memory footprint, we forego a reordering that enables the use of SSE instructions and improves cache performance, which was implemented in [16]). Figure 3.3 shows that using a single CPU core plus the GPU yields a runtime that is 9.5x shorter than with just one CPU core, which is quite encouraging considering that only the P2P step is offloaded to the GPU. The performance using multiple threads and the GPU is here 26x faster than the single-threaded CPU-only code.

In Figure 3.3, we also see that using the full CPU plus the GPU gives a performance that is 4.2x faster than using only the CPU, so adding one GPU to the system is equivalent to adding at least three CPU sockets in this implementation, assuming perfect speedup on the CPU. Using the GPU instead of additional CPUs, we avoid hitting the memory bandwidth limit and benefit from the higher floating point capabilities of the GPU.

The performance measurements described above were made using the harmonic potential $G(x_i, x_j) = -m_j/(x_i - x_j)$, where x_i and x_j are complex numbers. We also implemented the computationally more expensive logarithmic potential, used for example in computer graphics when plotting isopotentials. The additional arithmetic

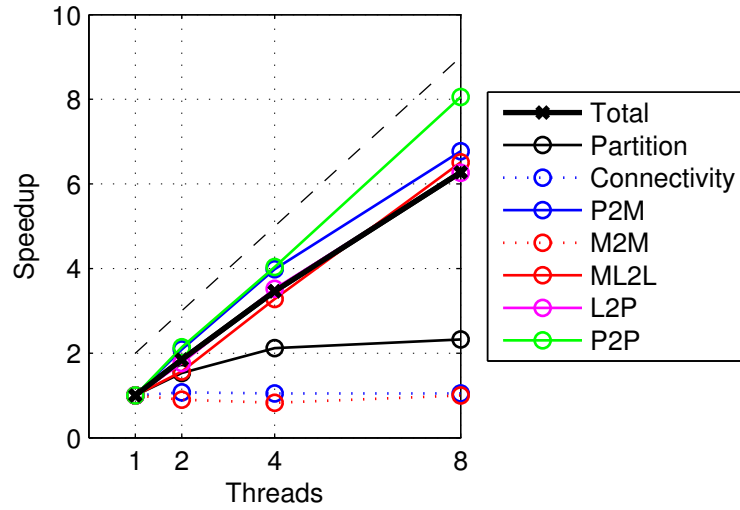


FIGURE 3.2. Strong scaling using only CPU, after tuning. Phases represented by dotted lines were not parallelized.

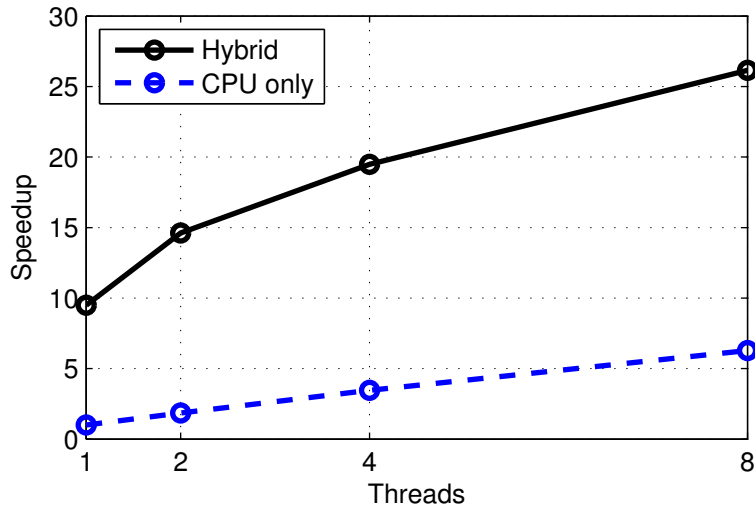


FIGURE 3.3. Comparison of CPU/GPU-hybrid and CPU-only speedup versus 1 CPU-only thread.

intensity of the logarithmic kernel improves the efficiency of our results because of better amortization of data transfer costs and kernel launch times on the GPU, and also for better cache performance on the CPU. Using the logarithmic potential, the CPU+GPU performance is 6x faster than using just the CPU, and the full system performance is 40x faster than our single-threaded CPU-only performance.

4. AUTOTUNING

Our autotuning scheme continuously measures the performance of relevant FMM subtasks and makes autotuning decisions for two performance-critical parameters in the FMM algorithm. Here, the only crucial assumption is that the FMM is used in a time-marching or iterative context. For most N -body problems, this is indeed the case. No parameters estimating the complexity of subtasks or computer system specifics need to be specified by the user.

The algorithmic complexity of the main program phases, as determined by θ and N_{levels} , was described in Section 2.3. For a given relative error tolerance TOL and θ , we use the result from [15] that $p \propto \log \text{TOL} / \log \theta$ to choose an expansion degree p to satisfy the required tolerance. This lets us use θ as a performance-tuning parameter while maintaining an error tolerance appropriate to the problem. Table 4.1 gives a sense of the range of p .

TOL	θ				
	0.35	0.4	0.5	0.6	0.65
10^{-6}	11	13	17	24	28
10^{-7}	14	16	21	28	34
10^{-8}	16	18	24	33	39

TABLE 4.1. Expansion degree p for sample values of TOL and θ (harmonic potential).

Roughly speaking, the CPU-part that is executed concurrently with the GPU-part is dominated by the downward pass, the runtime of which decreases as the runtime of the GPU-part increases. This opens up for an “*Extremum Control*”-approach [2, Chap. 13.3] where these two parameters are varied dynamically to remain close to the optimal choice. Clearly, controlling θ and N_{levels} also controls the load-balance between the CPU and GPU. Intuitively, this is desirable because we can ensure maximum utilization of the available hardware. As we will see, however, maximum utilization does not necessarily correspond to minimal runtime.

4.1. Static tuning. Before we can describe our approach to autotuning in more detail, the effects of parameter selection and particle distribution on the performance of our FMM implementation need to be clarified. We divide the performance-critical components of the code into three distinct sections; the M2L phase, consisting of the downward pass through the tree; the P2P phase, which consists of the direct evaluations in the near field; and the Q phase, which consists of the rest of the program. This division allows us to write the runtime of the hybrid code $\tilde{C}_{\text{hybrid}}$ and the CPU-only code \tilde{C}_{CPU} for a given problem as functions of θ and N_{levels} in the following way:

$$(4.1) \quad \tilde{C}_{\text{hybrid}}(\theta, N_{\text{levels}}) = \max(\tilde{C}_{\text{M2L}}(\theta, N_{\text{levels}}), \tilde{C}_{\text{P2P}}(\theta, N_{\text{levels}})) + \tilde{C}_{\text{Q}}(\theta, N_{\text{levels}}),$$

and

$$(4.2) \quad \tilde{C}_{\text{CPU}}(\theta, N_{\text{levels}}) = \tilde{C}_{\text{M2L}}(\theta, N_{\text{levels}}) + \tilde{C}_{\text{P2P}}(\theta, N_{\text{levels}}) + \tilde{C}_{\text{Q}}(\theta, N_{\text{levels}}).$$

The runtime of the M2L phase is given by $\tilde{C}_{\text{M2L}}(\theta, N_{\text{levels}}) = AC_{\text{M2L}} + B$ for some constants A, B (see (2.7)), and similarly for \tilde{C}_{P2P} (see (2.6)). From the complexity

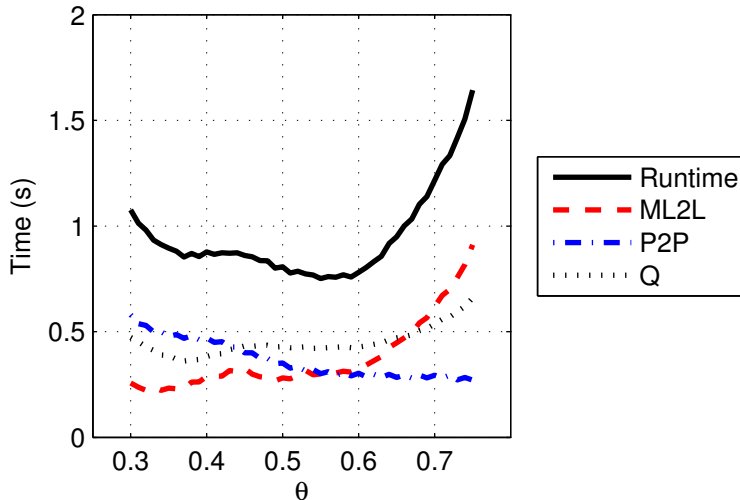


FIGURE 4.1. Runtime of hybrid code and the components M2L, P2P, and Q with varying θ . Note the saw-tooth pattern in M2L, P2P, and total runtime, and also the “central hump” behavior in M2L and Q. Simulation performed with 8 CPU-threads, $N = 10^6$ and a uniform square particle distribution.

analysis in Section 2.3 it is reasonably clear that at least one minimum $(\theta, N_{\text{levels}})$ exists, but the precise location depends on hardware, implementation, and problem specifics.

When considering the computational work for the M2L, P2P, and Q phases, it seems an attractive idea to tune $\tilde{C}_{\text{hybrid}}$ such that the CPU and GPU parts are balanced, $\tilde{C}_{\text{M2L}}(\theta, N_{\text{levels}}) \approx \tilde{C}_{\text{P2P}}(\theta, N_{\text{levels}})$, ignoring the small and nearly constant runtime for the Q phase. However, once M2L is parallelized and P2P is efficiently off-loaded to the GPU, Q becomes relatively large and this strategy is not optimal (see Figure 4.1). Therefore, we did not consider using load-balance information to tune θ , but only N_{levels} . Being run on an accelerator, P2P does not scale down with small problems because of PCI latency and kernel startup time, so for small problems, P2P is relatively constant. This means that optimal tuning for small problems puts a seemingly disproportionate amount of work on the GPU, because the time saved on performing Q on very small trees is greater than the increase in time spent on P2P. This also means that the performance gain of the GPU is smaller on small problems.

To study how particle distribution affects performance and tuning we have run the same experiment as in Figure 4.1, but this time with particles distributed approximately along a line. This scenario can for example be found in interface simulations and long Karman streets, as well as the vortex instability simulation that we present in Section 5.1. The specific effects of changing particle distributions depends on problem size, interaction potential, and machine specification, but it is worth pointing out that tuning for the wrong distribution can lead to poor performance. The computations for the linear distribution (Figure 4.2) ran most efficiently with $\theta = 0.49$, while the uniform distribution ran most efficiently with

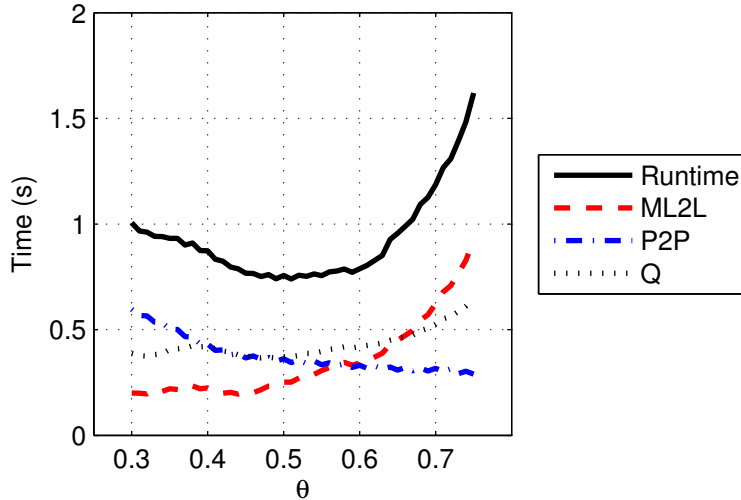


FIGURE 4.2. Runtime of line-like distribution. Note the “shallower” and left-shifted minimum compared to the uniform distribution.

$\theta = 0.55$. Running the uniform distribution with $\theta = 0.49$ would yield a performance penalty of 7%. In our experience, the optimal value of θ may lie anywhere in the range $[0.35, 0.65]$ and the potential performance penalty for values in this range often exceeds 30%. This motivates the use of dynamic autotuning.

The reason why optimal performance and maximum utilization do not always coincide is made clear in Figures 4.1 and 4.2. Maximum hardware utilization occurs when the M2L curve crosses the P2P curve. Depending on where this balance occurs, the runtime cost of lower utilization can be offset by savings in Q .

4.2. Dynamic Autotuning. The goal of autotuning is to achieve optimal performance while maintaining *generality* (applicability to many problems and situations), *robustness* (overcoming pathological conditions), *speed* (quickly finding the optimum), and *efficiency* (minimizing any additional computational work).

Generality is achieved by making as few assumptions as possible on the system we try to control. The main assumption here is that each iteration is a small incremental change compared to the previous one such that the observed response in performance is due to tuning attempts and not to the evolution of input data. Clearly, this assumption is necessary in order to use the runtime per iteration to evaluate the effectiveness of tuning parameters. A system which drastically changes is problematic to control simply due to poor estimation of the efficiency of the tuning steps.

A robust autotuner must be able to handle a number of potential pitfalls. Here we identify and describe some of the difficulties that we encountered in devising the autotuning for our FMM implementation.

4.2.1. Noise. Runtime measurements can vary for a multitude of reasons that are unrelated to the actual tuning efficiency. Runtime variation that is not attributable to changes in problem configuration or in tuning parameters is called *noise*. The

presence of noise necessitates taking repeated measurements. True repetition would involve freezing the problem state for several calls to the FMM-routine, but this would be prohibitively expensive. Instead, we assume that problem configuration changes sufficiently slowly and use the minimum runtime from a short sequence of iterations when making tuning decisions.

4.2.2. Multiple local minima. As Figure 4.1 shows, multiple local minima in runtime may exist. We have seen two large near-optimal regions, spaced widely apart in θ , as well as a saw-tooth profile when taking small steps in θ . An autotuner can get stuck at suboptimal parameter values even when tuning a relatively static problem. The reason for the two large near-optimal regions has been difficult to analyze in detail, but is likely related to the way θ is linked both to the number of expansion coefficients and connectivity pattern for multipole boxes. The saw-tooth pattern is similarly difficult to analyze conclusively, but we speculate that it is caused by discretization effects on the cache or shared memory efficiency of the M2L and P2P routines. Below, we present how the problem of multiple local minima can be solved using techniques from global optimization.

4.2.3. Discontinuous movement of the global minimum. When the problem configuration shifts the relative efficiency of two large near-optimal regions, the global optimum may move from the one to the other. Capturing such an event exactly requires knowledge of the performance of the entire range of θ at every iteration, so we need a heuristic rule that is efficient and not too costly.

4.2.4. Correlated controls. If there are two (or more) tuning parameters, there exists the possibility that each parameter cannot be tuned independently of the other. For the tuning to improve, *both* parameters must be adjusted at once. However, both our static analysis and experiments show that the optima in θ and N_{levels} are in practice almost completely independent.

In order to avoid creating an excessively complicated and application-specific scheme, we developed and evaluated a series of autotuning techniques, each of which addresses a particular issue, finishing with a robust autotuning system suitable for use in applications (see Section 5). The common design principle is that each method periodically attempts a change in a parameter (which we call a move), which is either accepted or rejected depending on the performance in the following time-steps.

4.2.5. AT1: Random walk. The simplest and most general autotuner performs a straightforward biased random walk. For each parameter, moves are generated in regularly spaced intervals as steps in a randomly selected direction. A pseudocode description is provided in Algorithm 1, where `timei` and `pi` are the runtime and the parameter configuration of the *i*th FMM call. `thetastep` is the unit length of a move in the θ parameter and is set to 0.01 unless otherwise specified and `randbit` is either 0 or 1, chosen randomly and with equal probability.

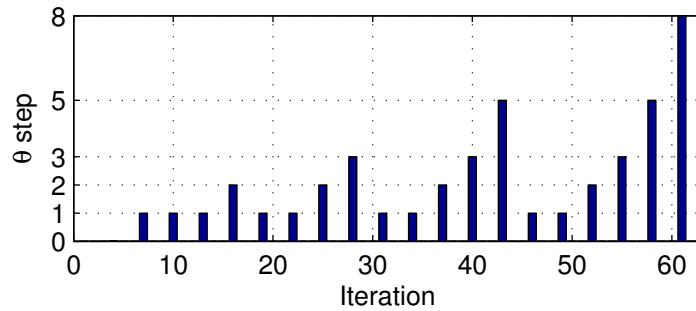
4.2.6. AT2: Directed walk with varying step size. A simple improvement is to remember the previous step. Moves are generated in the same direction if the previous move was successful, otherwise in the opposite direction. This method avoids moves in the wrong direction, but it can get stuck in a local minimum such as the ones observed in the static tuning experiments (Section 4.1). In the pseudocode of Algorithm 2, `move` represents a two dimensional direction in parameter space.

Algorithm 1: AT1: Random walk

```

if  $\text{time}_i > \text{time}_{i-1}$  then
    return  $p_{i+1} = p_{i-1}$  {Reject previous move}
end if
if time to move in  $N_{\text{levels}}$  then
    return  $p_{i+1} = [\theta, N_{\text{levels}} + (2 \cdot \text{randbit} - 1)]$ 
else if time to move in  $\theta$  then
    return  $p_{i+1} = [\theta + (2 \cdot \text{randbit} - 1) \cdot \text{thetastep}, N_{\text{levels}}]$ 
else
    return  $p_{i+1} = p_i$ 
end if

```

FIGURE 4.3. Progression of θ step length.

In order to avoid the problem of getting stuck in a local minimum when tuning θ , we introduce a growing step size when an apparent optimum is reached. For this to be effective, the step size must not grow too slowly, but growing the step size too rapidly can cause the algorithm to attempt big, large-grained, and expensive steps too often. Furthermore, in order to track a moving optimum closely, most step sizes must be small. We chose to use a sequence of steps which cycles through the Fibonacci sequence (see Figure 4.3). In the description of Algorithm 2, the function $\text{fib}(n)$ returns the n th Fibonacci number, and the counter fibcount is initialized to 1. Each time the end of a sequence is reached without accepting a move, the counter is reset and the length of the sequence, fiblength , is increased. For our applications, this extension has not been necessary, as AT1 already successfully avoids getting stuck in local minima, but it induces a negligible cost and is potentially very useful.

4.2.7. *AT3a: Loadbalance-aware directed walk with varying step size.* Intuition tells us that good hardware utilization yields good performance. This information can be included in an autotuner that generated moves in N_{levels} that always moves the loadbalance towards zero. Note that for CPU-only runs, this method is equivalent to AT2.

Another approach for determining the correct step direction for N_{levels} would be to use a scaling model that, based on the FMM's algorithmics, would predict the change in workloads for the CPU and the GPU. We did not pursue this approach, first because it is too application specific, and second because of the difficulty

Algorithm 2: AT2: Directed walk with varying step size

```

if  $\text{time}_i > \text{time}_{i-1}$  then
  if previous move was a  $\theta$ -move then
    if  $\text{fibcount} < \text{fiblength}$  then
      set  $\text{thetastep} = \text{fib}(\text{fibcount} + +)$ 
    else
      set  $\text{thetastep} = \text{fib}(\text{fibcount} = 1)$ 
      set  $\text{fiblength}++$  {Grow sequence}
    end if
    set  $\text{thetadir} = -\text{thetadir}$  {Reverse direction}
  else
    set  $\text{Nldir} = -\text{Nldir}$  {Reverse direction}
  end if
  return  $p_{i+1} = p_{i-1}$  {Reject previous move}
end if
if time to move in  $N_{\text{levels}}$  then
  set  $\text{move} = [0, 1] \cdot \text{Nldir}$ 
else if time to move in  $\theta$  then
  set  $\text{move} = [\text{thetastep}, 0] \cdot \text{thetadir}$ 
else
  set  $\text{move} = [0, 0]$ 
end if
return  $p_{i+1} = p_i + \text{move}$ 

```

in incorporating hardware- and problem-specific performance parameters into a model based on algorithmics. For example, cache and memory bus behavior can dramatically affect both the CPU and the GPU workload.

4.2.8. *AT3b: Directed walk with varying step size and cost estimation.* In this final version of autotuning, the user specifies `cap`, a maximum cost for the autotuning of N_{levels} . When a move is made that degrades performance, the next move in the same direction is scheduled so that the expected runtime cost is less than the specified maximum cost. The expected cost is based on the difference between the runtime of the rejected step and the runtime of the most recent accepted step. Cost estimation has two benefits: it prevents the cost for the autotuning to grow out of bounds, and since the test frequency increases near switching points it captures these almost exactly.

5. APPLICATIONS

In this section, we illustrate the behavior of our autotuning implementation by presenting results for three example applications with different properties. The numerical experiments were performed on single GPU-equipped nodes on a cluster. Each node is equipped with two 8-core AMD Opteron 6220 (Bulldozer) processors configured with 8 floating-point units in total and an Nvidia Tesla M2050 GPU. Timing measurements reported are the full iteration times or complete simulation times, as noted. Unless otherwise noted, the relative error tolerance is set to 10^{-6} (see Table 4.1 for the number of expansion coefficients).

Algorithm 3: AT3a: Loadbalance-aware directed walk with varying step size

```

if timei > timei-1 then
  if previous move was a  $\theta$ -move then
    if fibcount < fiblength then
      set thetastep = fib(fibcount + +)
    else
      set thetastep = fib(fibcount = 1)
    end if
    set thetadir = -thetadir {Reverse direction}
  end if
  return pi+1 = pi-1 {Reject previous move}
end if
if time to move in Nlevels then
  if CPU waits on GPU then
    set move = [0, 1] {More work on the CPU}
  else
    set move = [0, -1] {More work on the GPU}
  end if
else if time to move in  $\theta$  then
  set move = [thetastep, 0] · thetadir
else
  set move = [0, 0]
end if
return pi+1 = pi + move

```

5.1. **Vortex instability.** This problem involves a set of vortices, which are propagated with the flow velocity according to

$$(5.1) \quad \frac{dx_k}{dt} = \frac{1}{2\pi i} \sum_{k=1}^N \frac{\Gamma_i}{\bar{x} - \bar{x}_k} g_\delta(|x - x_k|)$$

where N is the number of vortices, x_k is the vortex positions (\bar{x}_k denotes the complex conjugate of x_k), Γ_i is the vortex strengths, and $g_\delta(r)$ is the Gaussian smoother with radius δ ,

$$(5.2) \quad g_\delta(r) = 1 - \exp\left(-\frac{r^2}{\delta^2}\right),$$

which is applied to avoid divergence as $x \rightarrow x_k$. The propagation is carried out using the Euler forward scheme. At the initial time, all vortices are located regularly in a long and relatively thin rectangle, with the upper half of the vortices given the opposite strength of the lower half (hence the sum of all circulations is zero). This setup creates a velocity shear field, which is an unstable configuration very similar to a Kelvin-Helmholtz instability. The simulation starts with a homogeneous distribution and evolves toward a more clustered distribution. This affects the number of connections in the near field of the interaction lists since the clustered distribution has a much larger variation in box-sizes.

5.1.1. *Evaluating the autotuners.* We ran the vortex instability simulation with each of our autotuners, as well as with a constant initial setting, to characterize the

Algorithm 4: AT3b: Directed walk with varying step size and cost estimation

```

if  $\text{time}_i > \text{time}_{i-1}$  then
  if previous move was a  $\theta$ -move then
    if  $\text{fibcount} < \text{fiblength}$  then
      set  $\text{thetastep} = \text{fib}(\text{fibcount} + +)$ 
    else
      set  $\text{thetastep} = \text{fib}(\text{fibcount} = 1)$ 
    end if
    set  $\text{thetadir} = -\text{thetadir}$  {Reverse direction}
  else
     $\text{cost} = \text{time}_i - \text{time}_{i-1}$ 
    if  $N_{\text{ldir}} > 0$  then
       $\text{upcost} := \text{upcost} + \text{cost}$  {cost of misstep}
       $\text{uptime} := (\text{upcost} + \text{cost})/\text{cap} - \text{basetime}$  {time to next up move}
       $\text{upinterval} := \text{uptime} \cdot i/\text{basetime}$  {# iterations to next up move}
    else
      {same logic for decreasing  $N_{\text{levels}}$ :}
       $\text{downcost} := \text{downcost} + \text{cost}$ 
       $\text{downtime} := (\text{downcost} + \text{cost})/\text{cap} - \text{basetime}$ 
       $\text{downinterval} := \text{downtime} \cdot i/\text{basetime}$ 
    end if
  end if
  return  $p_{i+1} = p_{i-1}$  {Reject previous move}
else
  set  $\text{basetime} = \text{basetime} + \text{time}_i$ 
end if
if time to move in  $N_{\text{levels}}$  then
  set  $\text{move} = [0, \pm 1]$  as appropriate
else if time to move in  $\theta$  then
  set  $\text{move} = [\text{thetastep}, 0] \cdot \text{thetadir}$ 
else
  set  $\text{move} = [0, 0]$ 
end if
  return  $p_{i+1} = p_i + \text{move}$ 

```

effectiveness of our autotuning schemes. Two problem sizes were used to illustrate how the autotuners' efficiency varies according to problem specifics. For the large problem, the initial value of N_{levels} was set to one less than optimal, which is a common scenario for example when stepping up from a small prototype to a full-scale production run. Table 5.1 shows that for large problems, all autotuners are able to realize significant performance improvements compared to an untuned run. We also see that AT3b performs slightly better than the other three schemes. In the small run, constant factors dominate runtime and tuning makes little difference. Here, AT3a makes costly tuning attempts in the wrong direction and the performance is 2.5% worse than for the untuned case. In the rest of the paper, we use AT3b

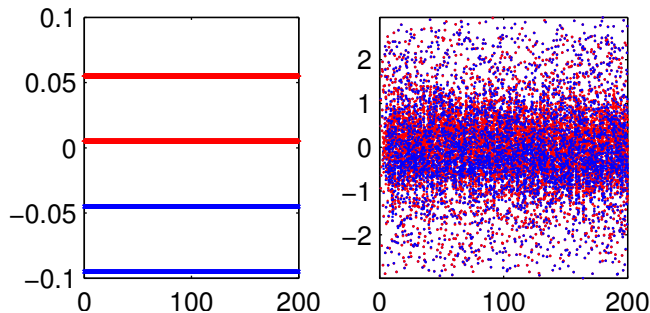


FIGURE 5.1. Distribution of points in vortex instability simulation at initialization and after 250 time-steps.

unless otherwise specified. This tuning scheme fulfills the requirements specified in Section 4.2 better than the other candidates.

Scheme	none	AT1	AT2	AT3a	AT3b
Small	1	1.02	1.05	0.97	1.07
Large	1	2.43	2.48	2.47	2.51

TABLE 5.1. Relative speedup of smaller ($N = 16000$) and larger ($N = 1.5$ million) vortex instability simulations using different tuning schemes.

5.2. Rotating galaxy. A two dimensional version of Newton’s law of gravitation states that the gravitational force felt by a particle i from a particle j of mass m_j is given by

$$(5.3) \quad F_{ij} = \frac{Gm_j}{r_{ij}},$$

where G is the gravitational constant and r_{ij} is the distance between the particles.

Equation (5.3), as written, contains a singularity as $r_{ij} \rightarrow 0$, so a smoother is applied that prevents the velocity for close particles from blowing up;

$$(5.4) \quad F_{ij} = \frac{Gm_j}{\sqrt{\delta^2 + r_{ij}^2}},$$

with δ a smoothing radius.

In this simulation, 3×10^5 particles with equal mass are placed uniformly in a disc and are given a velocity to start rotating as a rigid body about the center of mass. The force acting on each particle is calculated via the FMM with an error tolerance of 3×10^{-8} , and its velocity and position is updated with the velocity Störmer-Verlet method [18, Chap. 3.1]. As the simulation evolves, the distribution of particles within the disc becomes clustered and the structure begins to resemble an elliptic galaxy, see Figure 5.2.

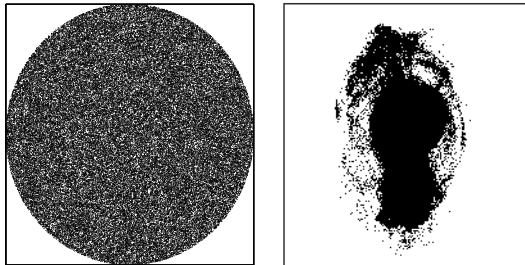


FIGURE 5.2. Distribution of points on disc in galaxy simulation at initialization and after 3000 time-steps.

5.2.1. *Initial tuning parameters.* The importance of choosing initial tuning parameters is the most apparent when running a short, relatively static simulation. Our galaxy simulation is therefore well-suited for a study of the initial tuning if we simulate a small number of time-steps. In Table 5.2, we present the relative runtime of the simulation with 300 time-steps for different sets of initial parameters. Because of the coarse granularity and big marginal effect on program speed, the optimal value of N_{levels} is found very quickly compared to the optimal θ (see Figures 5.3 and 5.4).

Due to the small number of iterations and the large size of the problem, this simulation is highly sensitive to bad initial tuning. We can therefore consider these results to be a worst-case scenario and expect that most simulations will experience a smaller impact due to initial choices of parameters.

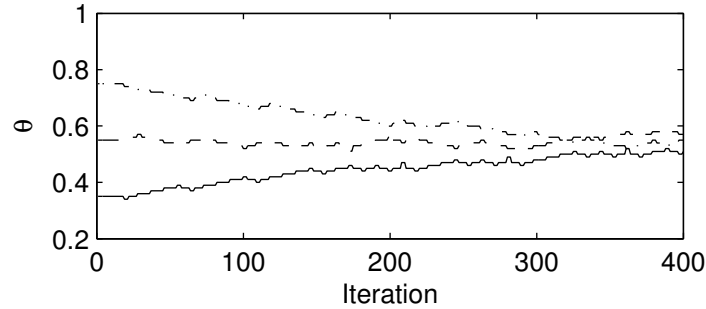
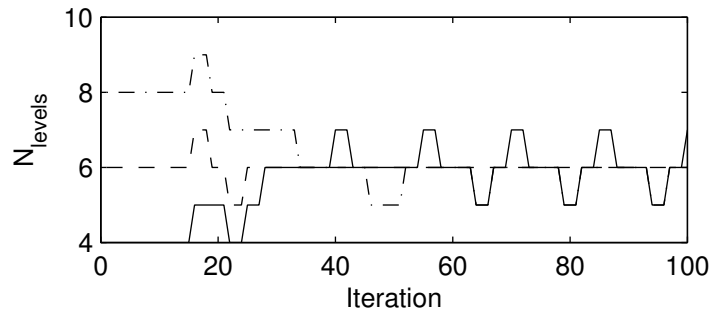
θ, p	N_{levels}			
	4	5	6	7
0.35, 14	1.16	1.05	1.02	1.03
0.55, 25	1.10	1.03	1	1.04
0.75, 54	1.13	1.07	1.32	1.46

TABLE 5.2. The total runtime of a 300 time-step galaxy simulation with different initial tuning parameters. Time is normalized to the fastest total runtime. p is the initial number of multipole coefficients. The relative error tolerance was set to 3×10^{-8} .

5.3. **Impulsively started flow around a cylinder.** A vortex method was used to simulate the flow around a rotating cylinder (peripheral speed one half the asymptotic flow velocity). This method is based on the vorticity equation [10], which is obtained by calculating the rotation of Navier Stokes Equations. For two dimensional incompressible flow, the equation can be written as

$$(5.5) \quad \frac{\partial \omega}{\partial t} + (\vec{V} \cdot \nabla) \omega = \nu \nabla^2 \omega.$$

This equation is discretized using point vortices with positions \vec{x}_k and strengths Γ_k , which moves freely with the flow. The equation is separated into two steps,

FIGURE 5.3. Evolution of θ for three different starting conditions.FIGURE 5.4. Evolution of N_{levels} for three different starting conditions. Note that the horizontal scale is shorter than in Figure 5.3.

where in the convection step, the particle positions are calculated according to

$$(5.6) \quad \frac{d\vec{x}_k}{dt} = \vec{V}_k$$

and in the diffusion step, the vorticity is updated;

$$(5.7) \quad \frac{d\omega}{dt} = \nu \nabla^2 \omega.$$

The diffusion step is implemented using the vorticity redistribution method (VRM) [22]. The diffusion algorithm was also used to merge close vortices as this can be done in the VRM by forcing the circulation of a vortex to zero. This was performed every 10th step and causes the regions with vorticity to have a quite homogeneous distribution of vortices. The total distribution of vortices was therefore characterized by regions with either a homogeneous vortex distribution, or no vortices at all, see Figure 5.5. The no slip boundary conditions was solved by adding a line of vortices at a distance of $\sqrt{0.5\nu\Delta t}$ from the boundary and adapting the strength of these vortices to give zero tangential flow on the boundary. This method is similar to the suggested solution by Chorin [9] and is how vorticity is introduced into the flow.

The flow velocity is calculated using the method of images, which gives an analytical solution to the continuity equation for a cylinder flow [19]. Using complex

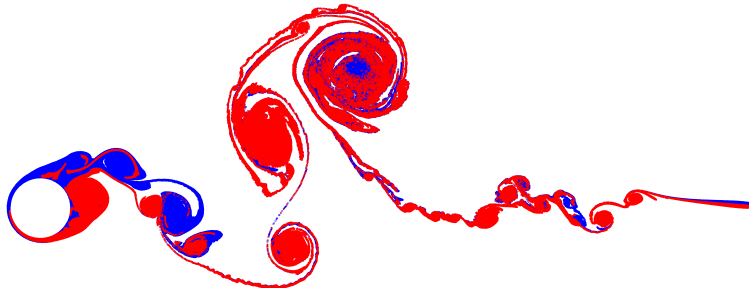


FIGURE 5.5. Sample vortex distribution for the rotating cylinder flow after 500 time steps.

numbers, the velocity V at position z is obtained as

$$(5.8) \quad V = V_\infty \left(1 - \frac{R^2}{x^2}\right) + \frac{1}{2\pi i} \sum_{k=1}^N \Gamma_i \left(\frac{g_\delta(|\bar{x} - \bar{x}_k|)}{\bar{x} - \bar{x}_k} - \frac{g_\delta\left(\left|\bar{x} - \frac{R^2}{x_k}\right|\right)}{\bar{x} - \frac{R^2}{x_k}} \right),$$

where $g_\delta(r)$ is the Gaussian smoother in (5.2). This expression includes the velocity contribution from all vortices at positions x_k (again, \bar{x}_k in (5.8) is the complex conjugate of x_k).

All interactions between the vortices are evaluated with the FMM. Due to the mirror vortices inside the cylinder, the amount of vortices is twice as many as the number of evaluation points. The mirror vortices are very densely packed inside the cylinder, and especially so close to the cylinder center. Although our particular implementation only applies for a cylinder, by using conformal mappings the technique with mirror vortices can be used to simulate other geometries as well [12, 13].

The convection step is carried out using the fourth order Runge-Kutta method, while the diffusion step is handled in a single step using the $O(\Delta t)$ method described in [22]. The higher order for the convection (compared to diffusion) is motivated by the fact that the problem is convection dominated for high Reynolds number and that increasing the VRM order is computationally very expensive.

The simulations were performed for an impulsively started flow, meaning that there were no vortices at the first time-step. The Reynolds number for the simulation was chosen to be 10000.

Since both the distribution geometry as well the number of particles varies greatly during this simulation, it can be considered a stress test of our implementation and the auto-tuning schemes.

5.3.1. *Capping the tuning cost.* AT3b allows the user to arbitrarily select `cap`, the maximum expected cost of tuning N_{levels} . If `cap` = 0, no tuning of N_{levels} is done, while if `cap` is large enough, N_{levels} is adjusted every time-step. In Figure 5.6, we have repeated the flow simulation with varying `cap`. The proportional rise in simulation runtime after about `cap` = 0.1 suggests that, even for a rapidly evolving simulation such as this, tuning need not cost more than 10% for it to accurately capture switching times in N_{levels} . For simulations that evolve more slowly, `cap` can be set lower, between 5–10%. To give a feeling for how `cap` affects the tuner's

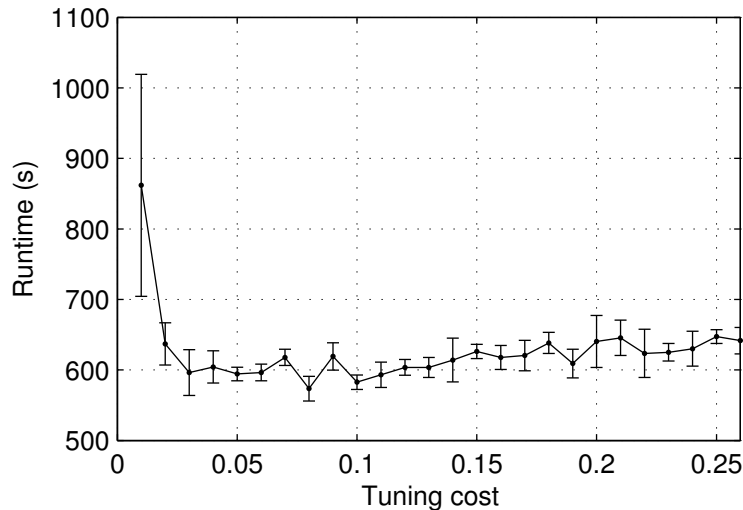


FIGURE 5.6. Runtime of cylinder flow simulation for 400 time-steps using AT3b with varying maximum tuning cost (cap). The simulation was repeated 5 times for each tuning cost, and the error bars indicate one standard deviation.

behavior, Figure 5.7 shows the value of N_{levels} and θ over time with $\text{cap} = 4\%$ and 12% .

6. CONCLUSIONS

In this paper we have presented a variant of the FMM and shown that it can be efficiently adapted for parallelization on hybrid computer systems, exploiting both multiple threads and an accelerator. We base the parallel FMM scheme on the heterogeneity in the algorithm, and by using a dynamic autotuning technique our implementation can exploit systems with different hardware characteristics and adapt to different problem settings without the need for explicitly modifying computer architecture- or problem-dependent parameters.

We also come to several other conclusions that we believe are of fairly general character. Firstly, optimal performance can generally not be expected when a heterogeneous computer is load balanced. In fact, we have shown that the degree of load *imbalance* can *at best* only be used as an indicator of where to look for well-tuned and efficient core usage.

Secondly, a robust autotuning strategy which does not make strong complexity assumptions on the algorithm at hand will require a certain degree of heuristics. To some extent this observation is connected to the previous point since, if we cannot completely rely on the dynamically measured degree of load balance, then clearly some type of trial-and-error has to be employed.

Thirdly, if some design variables affect the performance more drastically than others, a performance budget strategy of some kind should be implemented. In the implementation reported here this was the case for the variable N_{levels} where the cost of varying this variable can be measured on the fly so as to avoid too frequent changes.

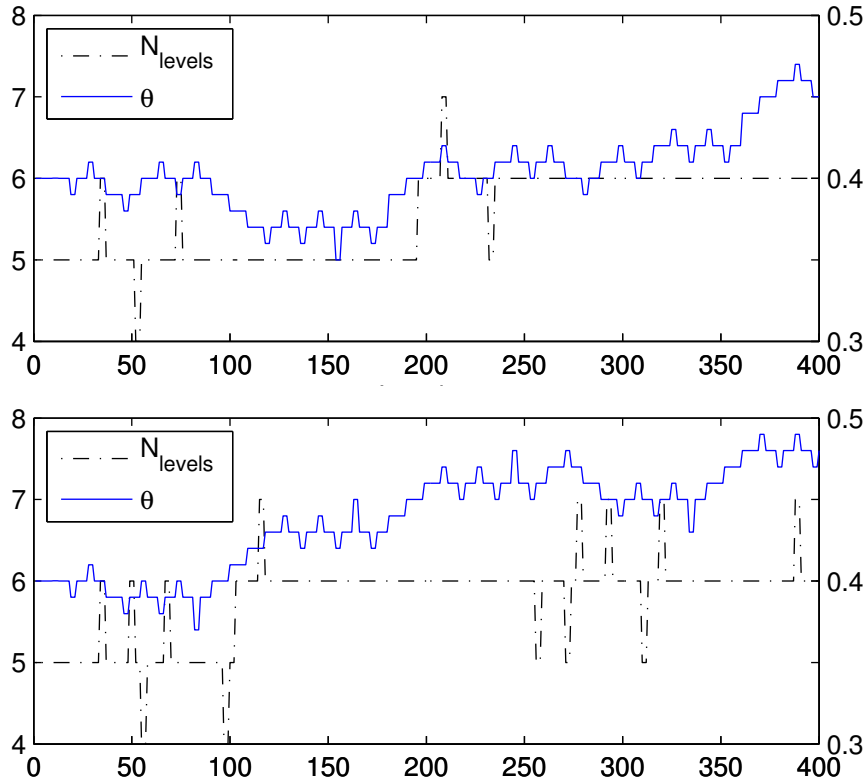


FIGURE 5.7. Timeseries showing evolution of N_{levels} and θ over the course of a cylinder flow simulation run. *Top*: Max tuning cost $\text{cap} = 4\%$, slightly too low to capture the optimal switching points. *Bottom*: $\text{cap} = 12\%$, slightly higher than necessary.

The utility of GPU-based accelerators is still a much-debated question in the scientific computing community. While an increasing proportion of large-scale computing machinery include GPUs, smaller university-level computers are still predominantly pure CPU machines, and typical desktop computers have GPUs that are more suited to media rendering than scientific applications. Our contribution to this debate is the transparent usage of one GPU, with a performance improvement that matches (or even exceeds) the performance one would expect from an expensive CPU upgrade. Table 6.1 gives the relative performance of our code with or without the GPU for each of our experiments. We see that the 4x speedup in the static experiment forms a reasonable upper limit of hybrid acceleration, and as expected this limit is only realized for sufficiently large problems.

6.1. Reproducibility. The FMM implementation described in this paper is available for download via the second author’s web-page¹. The code compiles both in a CPU-only version and in a hybrid version and comes with a convenient Matlab mex-interface. The hybrid version requires Cuda and an Nvidia GPU to function.

¹<http://user.it.uu.se/~stefane/freeware>

	Vortex instability	Galaxy	Cylinder flow
CPU (s)	425	1094	1451
CPU+GPU (s)	379	324	367
Speedup	1.12	3.37	3.95

TABLE 6.1. Performance comparison of CPU-only and hybrid code for the experiments conducted in the paper.

Along with the code, automatic Matlab-scripts that repeat the numerical experiments presented here are also distributed.

ACKNOWLEDGMENT

This work was financially supported by the Swedish Research Council within the UPMARC Linnaeus center of Excellence (M. Holm, S. Engblom, S. Holmgren) and the Swedish Energy Agency, Statkraft AS, Vinnova and Uppsala University within the Swedish Centre for Renewable Electric Energy Conversion (A. Goude).

REFERENCES

- [1] S. Aluru. Greengard’s N -body algorithm is not order N . *SIAM J. Sci. Comput.*, 17(3):773–776, 1996. doi:10.1137/S1064827593272031.
- [2] K. J. Åström and B. Wittenmark. *Adaptive Control*. Addison-Wesley Series in Electrical Engineering: Control Engineering. Addison-Wesley, Reading, MA, 1989.
- [3] C. Augonnet, S. Thibault, R. Namyst, and P.-A. Wacrenier. StarPU: A Unified Platform for Task Scheduling on Heterogeneous Multicore Architectures. *Concurrency and Computation: Practice and Experience, Special Issue: Euro-Par 2009*, 23:187–198, 2011. doi:10.1002/cpe.1631.
- [4] J. Barnes and P. Hut. A hierarchical $O(N \log N)$ force-calculation algorithm. *Nature*, 324(6096):446–449, 1986. doi:10.1038/324446a0.
- [5] G. Blelloch and G. Narlikar. A practical comparison of N -body algorithms. In *Parallel Algorithms*, volume 30 of *Series in Discrete Mathematics and Theoretical Computer Science*, 1997.
- [6] J. Carrier, L. Greengard, and V. Rokhlin. A fast adaptive multipole algorithm for particle simulations. *SIAM J. Sci. Stat. Comput.*, 9(4):669–686, 1988. doi:10.1137/0909044.
- [7] A. Chandramowlishwaran, S. Williams, L. Oliker, I. Lashuk, G. Biros, and R. Vuduc. Optimizing and tuning the fast multipole method for state-of-the-art multicore architectures. In *Parallel Distributed Processing (IPDPS), 2010 IEEE International Symposium on*, pages 1–12, 2010. doi:10.1109/IPDPS.2010.5470415.
- [8] H. Cheng, L. Greengard, and V. Rokhlin. A fast adaptive multipole algorithm in three dimensions. *J. Comput. Phys.*, 155(2):468–498, 1999. doi:10.1006/jcph.1999.6355.
- [9] A. J. Chorin. Numerical study of slightly viscous flow. *J. Fluid. Mech.*, 57:785–796, 1973.
- [10] G. H. Cottet and P. D. Koumoutsakos. *Vortex Methods: Theory and Practice*. Cambridge University Press, 2008.

- [11] F. A. Cruz, M. G. Knepley, and L. A. Barba. PetFMM—a dynamically load-balancing parallel fast multipole library. *Int. J. Numer. Meth. Engng.*, 85: 403–428, 2011. doi:10.1002/nme.2972.
- [12] P. Deglaire, O. Ågren, H. Bernhoff, and M. Leijon. Conformal mapping and efficient boundary element method without boundary elements for fast vortex particle simulations. *Eur. J. Mech. B Fluids*, 27(2):150–176, 2008.
- [13] P. Deglaire, S. Engblom, O. Ågren, and H. Bernhoff. Analytical solutions for a single blade in vertical axis turbine motion in two-dimensions. *Eur. J. Mech. B Fluids*, 28(4):506–520, 2009. doi:10.1016/j.euromechflu.2008.11.004.
- [14] W. Dehnen. A hierarchical O(N) force calculation algorithm. *J. Comput. Phys.*, 179(1):27–42, 2002.
- [15] S. Engblom. On well-separated sets and fast multipole methods. *Appl. Numer. Math.*, 61(10):1096–1102, 2011. doi:10.1016/j.apnum.2011.06.011.
- [16] A. Goude and S. Engblom. Adaptive fast multipole methods on the GPU. *J. Supercomput.*, 63(3):897–918, 2013. doi:10.1007/s11227-012-0836-0.
- [17] L. Greengard and V. Rokhlin. A fast algorithm for particle simulations. *J. Comput. Phys.*, 73(2):325–348, 1987. doi:10.1016/0021-9991(87)90140-9.
- [18] M. Griebel, S. Knapek, and G. Zumbusch. *Numerical Simulation in Molecular Dynamics*, volume 5 of *Texts in Computational Science and Engineering*. Springer Verlag, Berlin, 2007.
- [19] L. Milne-Thomson. *Theoretical Hydrodynamics*. Dover Books on Physics Series. Dover Publications, 1968.
- [20] Nvidia. Cuda C Programming Guide. Available at <http://docs.nvidia.com/cuda/cuda-c-programming-guide/>, 2013.
- [21] L. Nyland, M. Harris, and J. Prins. *GPU Gems 3*, chapter 31. Fast N-Body Simulation with CUDA. Pearson Education, Inc., 2007.
- [22] S. Shankar and L. van Dommelen. A new diffusion procedure for vortex methods. *J. Comput. Phys.*, 127:88–109, 1996. doi:10.1006/jcph.1996.0160.
- [23] M. Tillenius and E. Larsson. An efficient task-based approach for solving the N-body problem on multicore architectures. In *PARA 2010: Applied Parallel and Scientific Computing*. University of Iceland, 2010.
- [24] R. Yokota. An FMM based on dual tree traversal for many-core architectures. *J. Algorithms & Comput. Tech.*, 7(3):301–324, 2013. doi:10.1260/1748-3018.7.3.301.
- [25] J. Zhu, Y. Lei, and J. Shan. Parallel FMM algorithm based on space decomposition. In *Grid and Cooperative Computing (GCC), 2010 9th International Conference on*, pages 168–173, 2010. doi:10.1109/GCC.2010.43.

(M. Holm, S. Engblom, and S. Holmgren) DIVISION OF SCIENTIFIC COMPUTING, DEPARTMENT OF INFORMATION TECHNOLOGY, UPPSALA UNIVERSITY, SE-751 05 UPPSALA, SWEDEN.
E-mail address: marcus.holm, stefan.engblom, sverker.holmgren@it.uu.se

(A. Goude) DIVISION OF ELECTRICITY, DEPARTMENT OF ENGINEERING SCIENCES, UPPSALA UNIVERSITY, SE-751 21 UPPSALA, SWEDEN.
E-mail address: anders.goude@angstrom.uu.se